Solar Physics (2023) 298:118
https://doi.org/10.1007/s11207-023-02212-8

RESEARCH

Repeated Type III Burst Groups Associated with a B-Class Flare and a Narrow-Width CME

Silja Pohjolainen[1] · **Derek McKay**[2,3] · **Nasrin Talebpour Sheshvan**[4] · **Christian Monstein**[5]

Received: 2 April 2023 / Accepted: 20 September 2023

Abstract
We have analysed a solar event from 27 September 2021, which included a small GOES B-class flare, a compact and narrow-width CME, and radio type III bursts that appeared in groups. The long-duration, repeated metric type III burst emission indicates continuous electron acceleration at high altitudes. The flaring active region was surrounded by strong magnetic fields and large-scale loops, which guided the outflow of the CME plasmoid and hence the narrow, bullet-like appearance of the CME. Radio imaging and EUV observations confirmed the direction of particle propagation and the depletion of matter from the solar source region. We observed V-shaped type III burst emission lanes, which also explain the field configuration and suggest a possible location for repeated reconnection that occurred at a constant altitude.

Keywords Flares · Dynamics · Magnetic fields · Corona · Radio bursts · Association with flares · Coronal mass ejections · Initiation and propagation

✉ S. Pohjolainen
silpoh@utu.fi

D. McKay
derek.mckay@aalto.fi

N. Talebpour Sheshvan
nasrin.talebpoursheshvan@utu.fi

C. Monstein
christian.monstein@irsol.usi.ch

1 Tuorla Observatory, Department of Physics and Astronomy, University of Turku, Turku, Finland

2 Present address: Aalto University Metsähovi Radio Observatory, Metsähovintie 114, FI-02540 Kylmälä, Finland

3 Finnish Centre for Astronomy with ESO (FINCA), FI-20014 University of Turku, Finland

4 Department of Physics and Astronomy, University of Turku, Turku, Finland

5 Istituto ricerche solari Aldo e Cele Daccò (IRSOL), Faculty of Informatics, Università della Svizzera italiana (USI), CH-6605 Locarno, Switzerland

Published online: 09 October 2023

1. Introduction

Solar flares are powerful bursts of energy release, often followed by coronal mass ejections (CMEs). These eruptions accelerate particles and eject plasma from the solar atmosphere (Benz, 2008; Gopalswamy, 2016). However, the relationship between flares and CMEs is not always clear (Kawabata et al., 2018). The most energetic flares are known to be associated with fast and wide CMEs, but the relation between CMEs and small and less energetic flares, or with flares missing altogether, is more complicated. It has been suggested that the magnetic reconnection process that happens beneath the CME affects the CME dynamics most (Vršnak, Sudar, and Ruždjak, 2005).

As flares and CMEs accelerate particles, some of their processes can be observed in radio emission; see reviews by Nindos et al. (2008) and Pick and Vilmer (2008). Particle streams, i.e. accelerated electrons, cause radio emission at the local plasma frequency as they propagate through the solar atmosphere. The radio emission is then also subject to scattering by density inhomogeneities and other propagation effects (Kontar et al., 2019). The most often observed solar radio emission types are type III bursts (caused by accelerated electron beams), type II bursts (caused by shock-accelerated electrons, typically ahead of propagating CMEs), and type I noise storms (electrons trapped in the magnetic field).

Type III bursts are most often associated with flares, and they can appear as isolated bursts or in groups. There is now direct evidence that semi-relativistic electrons energized in magnetic reconnection regions produce type III bursts (Cairns et al., 2018). At starting frequencies higher than 100 MHz, type III bursts have been found to be associated mostly with GOES B- and C-class flares, but the X-ray emission at 6 keV usually lasts much longer than the groups of type III bursts (Reid and Vilmer, 2017). Type III bursts can be observed as fast-drifting emission features in the radio dynamic spectra, some only at decimetric–metric wavelengths (coronal heights) and some continuing to kilometer waves (near Earth distances).

Shocks can form in the solar corona when an ejected projectile propagates at speed higher than the local magnetosonic speed. Also, flare blasts can create propagating shocks that accelerate electrons (Warmuth, 2007). The frequency drift in a radio type II burst is much slower than in type III bursts, as the drift compares to the propagation speed of the shock. Observationally, type II bursts can often be identified from their harmonic emission (Roberts, 1959).

Type I noise storms are associated with active regions and sometimes with flares and CMEs, but the typical duration of a noise storm continuum is significantly longer than that of the associated flare (Iwai et al., 2012). The broad-band continuum also contains short-duration, narrow-band bursts. The generally accepted scenario is that the emission is due to non-thermal electrons trapped in closed magnetic fields. The origin of these fast electrons is not very clear, but small-scale reconnection and weak shocks associated with newly emerging flux have been suggested; see, for example, Mercier et al. (2015) and references therein. Mondal and Oberoi (2021) recently suggested that small-scale reconnection may produce electron beams, which quickly get collisionally damped, and therefore the plasma emission occurs only within a narrow bandwidth.

In this study, we analyse a solar event that consisted of a small, GOES B-class flare and a compact CME that had a very narrow width and relatively high initial speed and was associated with groups of metric type III bursts and type I noise storm bursts. Our aim is to find out the reason for the continuous particle acceleration and the generation of repeated type III bursts. We also investigate the CME formation and its propagation as a compact, bullet-like form.

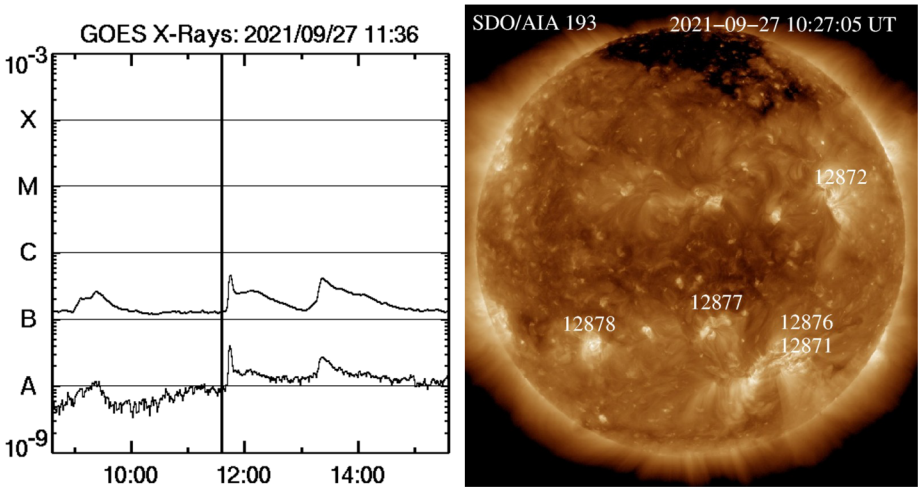

Figure 1 On 27 September 2021 a GOES B4.5-class flare was observed to start at 11:40 UT, with maximum flux at 11:46 UT, at location S29W35 in active region AR 12871.

2. Data and Analysis

We have used in the analysis extreme ultraviolet (EUV) solar images from the *Atmospheric Imaging Assembly* (AIA) instrument onboard the *Solar Dynamics Observatory* (SDO: Lemen et al., 2012) and from the *Extreme Ultraviolet Imager* (EUVI) onboard the *Solar Terrestrial Relation Observatory* (STEREO) spacecraft (Wuelser et al., 2004). Coronagraph images and associated data products were obtained from the CDAW LASCO CME Catalog at cdaw.gsfc.nasa.gov. The *Gamma-ray Burst Monitor* (GBM) onboard the *Fermi Gamma-ray Space Telescope* (Meegan et al., 2009) provided X-ray flux observations for the event.

For decimetric–metric radio emission, we used radio spectral data from the *Kilpisjärvi Atmospheric Imaging Receiver Array* (KAIRA: McKay-Bukowski et al., 2015) located in Finland, from the various CALLISTO instruments in the *e-Callisto* Network (Benz, Monstein, and Meyer, 2005; Monstein, Csillaghy, and Benz, 2023), and from the *Nançay Decameter Array* (NDA: Lecacheux, 2000) and ORFEES radio-spectrograph (Hamini et al., 2021) located in France and provided by the Radio Monitoring website at secchirh.obspm.fr. For longer radio wavelengths, we used data from the WAVES instrument on the *Wind* spacecraft (Bougeret et al., 1995). Radio imaging at selected frequencies in the 150 – 445 MHz range were provided by the *Nançay Radioheliograph* (NRH: Kerdraon and Delouis, 1997).

2.1. Active Region and Flare

A small, GOES B4.5-class flare was observed on 27 September 2021 (SOL2021-09-27T11:46) in NOAA active region (AR) 2871, located at S29W35 (Figure 1). The GOES flare was listed as starting at 11:40 UT, peaking at 11:46 UT, and ending at 11:50 UT. However, a post-burst increase was observed to last until 12:50 UT in the 1.5 – 12.5 keV energy range (1 – 8 Å). The potential magnetic field is presented in Figure 2, created using both SDO/AIA (Earth view) and STEREO-A/EUVI (separation angle between them 39.8 degrees) observations and the potential-field source-surface (PFSS) model.

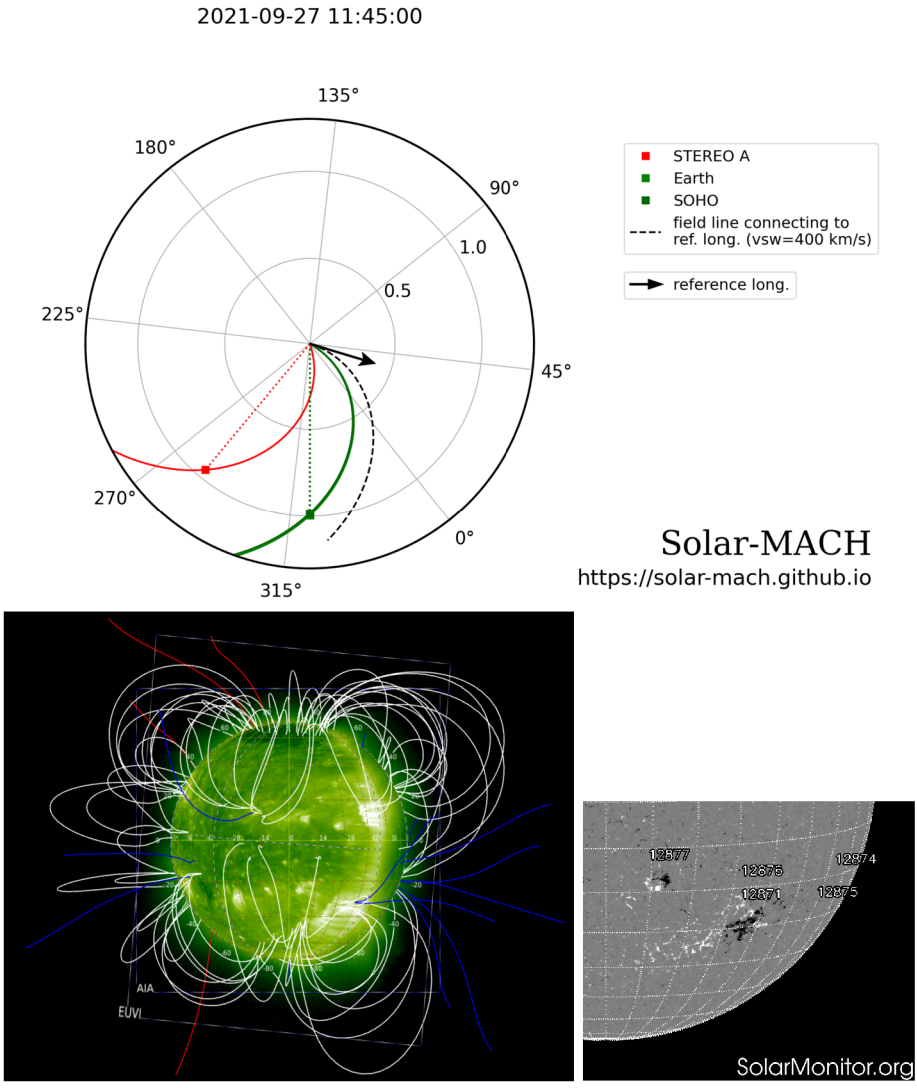

Figure 2 *Top*: Spacecraft locations on 27 September 2021. The STEREO-A spacecraft longitude separation to Earth was 39.8 degrees, with SOHO, SDO, *Wind*, and *Fermi* spacecraft at Earth's longitude. The reference longitude is for the B4.5-class flare located at S29W35. (Plot prepared with Solar-MACH, The Solar MAgnetic Connection HAUS tool.) *Bottom left*: STEREO-A/EUVI image rotated to SDO/AIA field of view, with PFSS magnetic field lines. *Blue and red lines* indicate open field with opposite polarities and *white lines* indicate closed field. *Bottom right*: SDO/HMI magnetogram of the eruption region (from SolarMonitor.org).

Fermi/GBM also observed the flare with its NaI detectors that cover the energy range from a few keV to about 1 MeV. In the 4 – 15 keV energy range the maximum count rates were observed during 11:43:50 – 11:44:40 UT, but count-rate enhancements were also visible at 11:43 UT, 11:44 UT, 11:46 UT, and 11:50 UT at energies 4 – 50 keV (Figure 5). Flare emission was observed until 11:51 UT, after which the spacecraft turned away from

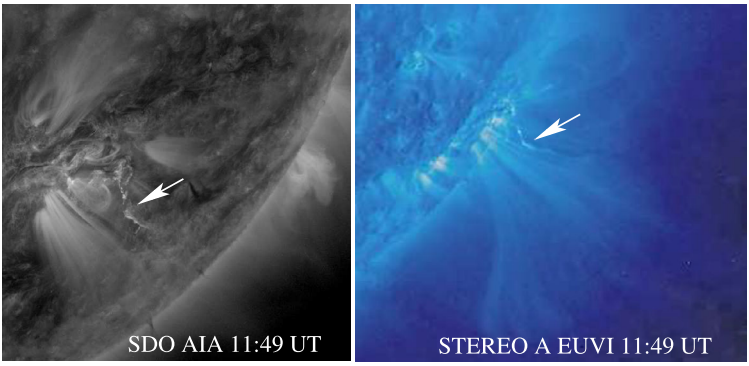

Figure 3 SDO/AIA and STEREO-A/EUVI images of the AR and its surroundings at 11:49 UT. *Arrow* points to the ejected filament/plasmoid structure. Note the bending of the structure along the magnetic field lines.

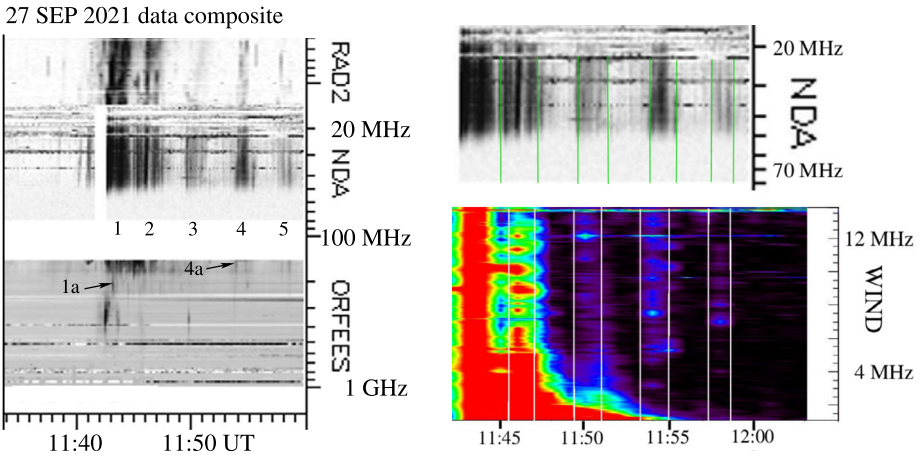

Figure 4 Radio Monitoring composite showing observed radio emission in the dynamic spectra for the 27 September 2021 event. Numbers 1 – 5 refer to the type III burst groups. The locations of bursts *labelled 1a and 4a* are shown in Figures 7 and 6, respectively. Comparison between NDA and *Wind*/WAVES spectra is also shown.

the Sun (*Fermi* is in low-Earth orbit). The comparison between X-rays and radio emission is discussed more in Section 2.2.

A plasmoid ejection was observed to start from the flare site at 11:42 UT. A narrow filamentary structure was ejected from the AR, and it was observed to change direction and turn to follow the fan-like magnetic field. The bending of this long filamentary structure along the magnetic field lines is shown in the EUV images from SDO and STEREO-A; see Figure 3. The bending was best observed in the STEREO-A view, over the limb and against the sky, which enabled us to better estimate and compare the source heights.

2.2. Radio Emission

The main radio features associated with the flare–CME event were type III bursts, i.e. fast electron beams propagating at speeds $\approx 0.3\,c$. Figure 4 shows how the type III

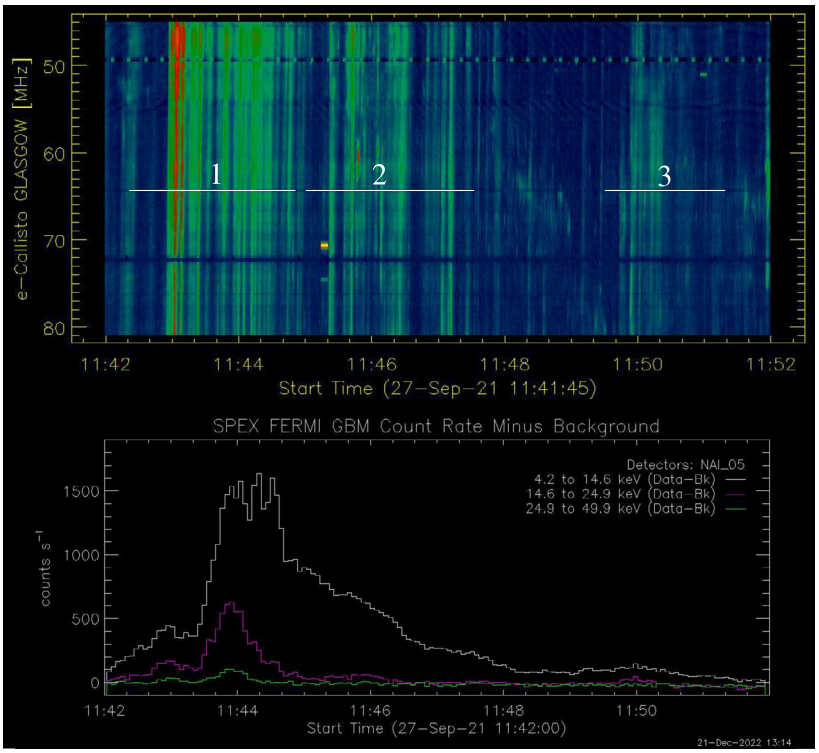

Figure 5 *Fermi*/GBM background-subtracted X-ray counts from the most sunward-pointing detector at 11:42 – 11:52 UT (*bottom*). The energy ranges are 4 – 15 keV, 15 – 25 keV, and 25 – 50 keV. Radio dynamic spectrum from e-CALLISTO Glasgow is shown on *top*, at frequency range 45 – 81 MHz. *Numbers and lines* indicate the type III burst groups and their durations.

bursts occurred in groups. We could identify five separate groups, labelled 1 – 5 in Figure 4. The approximate burst group durations were 11:42:20 – 11:44:50 UT (150 seconds), 11:45:00 – 11:47:35 UT (155 seconds), 11:49:30 – 11:51:20 UT (110 seconds), 11:53:50 – 11:55:20 UT (90 seconds), and 11:57:30 – 11:58:55 UT (85 seconds).

The type III burst groups appear to have some temporal association with the X-ray flux measured by *Fermi*/GBM (Figure 5). Intense type III burst emission is observed at the time of the first X-ray peak near 11:43 UT, and the end time of the first type III burst group is also the time when the X-ray burst intensity decreases. There is a small increase in X-rays during the type III burst group number 3. However, we find no clear one-to-one correspondence between the X-ray count rate peaks and individual type III bursts.

Bursts within the first two type III burst groups reached interplanetary space and propagated to Earth distances (emission continues down to kHz frequencies), but burst emission in the later three groups fades away at 5 – 2 MHz; see the *Wind*/WAVES dynamic spectrum in Figure 4.

Some isolated type III bursts were observed at 500 – 200 MHz near the flare start time, but most of the type III burst groups had a start frequency near 200 MHz (Figure 4). The start frequency, 200 MHz, corresponds to an atmospheric height of 0.15 $R_\odot$ when calculated with the 2-fold Newkirk atmospheric density model (Newkirk, 1961), which describes well the lower altitudes in the solar corona. Another often used atmospheric model, the so-called

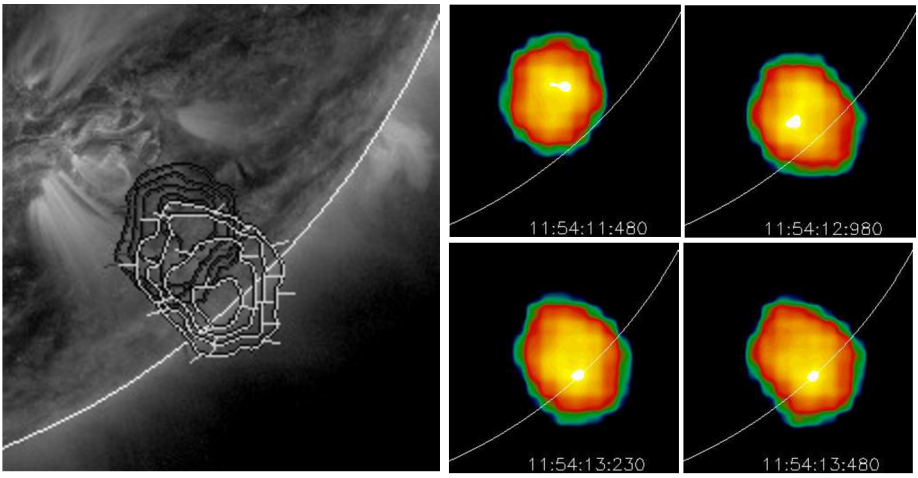

Figure 6 Temporal evolution of burst locations at 150 MHz, observed with NRH. The sources are shown near burst start (*black contours*) and burst end (*white contours*), overplotted on an EUV image (*left*). The spatial evolution is also shown in the color images, from 11:54:11 to 11:54:13 UT (*right*). This spectral feature is marked *4a* (within group 4 bursts) in Figure 4. The radio source locations are typical for all type III bursts in the type III burst groups observed at 150 MHz.

hybrid model by Vršnak, Magdalenič, and Zlobec (2004), gives heights close to the 2-fold Newkirk model in the low corona but works well also at larger distances. The differences between atmospheric density models and the calculation of radio source heights is explained in, e.g., Pohjolainen et al. (2007).

Individual type III bursts could be best identified in the 80 – 20 MHz frequency range, and many of them could be imaged near their start frequency, at 150 MHz with NRH. These bursts were all located south-west of the AR, and some of them reached the solar limb; see an example of radio imaging in Figure 6, the type III burst is marked 4a in the dynamic spectrum in Figure 4. The calculated source heights at 150 MHz are in agreement with the imaged radio source distances from the AR. As the imaged radio sources are observed on the solar disc in projection from the Earth view, their heights are only estimates and can also suffer from various plasma effects (Chen et al., 2020).

2.3. Specific Radio Spectral Features

Near the flare start, at 11:43 UT, a high-frequency type III burst was observed, and it could be imaged at 228 and 270 MHz. Two separate radio source locations appeared then, one south-west and one north of the AR (Figure 7). This type III burst is marked 1a in the dynamic spectrum in Figure 4. The flux measured from the northern source region showed an enhancement at 270 MHz, and it peaked later than the 228 MHz flux. This suggests that the type III burst was reversed, i.e. the electron beam was moving down in the solar atmosphere. We note that the northern source did not appear again at later times.

Some of the type III bursts showed enhanced plasma emission features along the electron-beam propagation path; the two features are indicated with arrows in Figure 8. The features appeared at $\approx$ 60 MHz around 11:46 UT. They were observed by *e-Callisto* stations and KAIRA, with different temporal resolutions of 0.25 and 0.01 seconds, respectively. The enhancements had a narrow bandwidth, only a few MHz, and on closer look they seem to be separated from individual type III emission lanes and have a curved appearance.

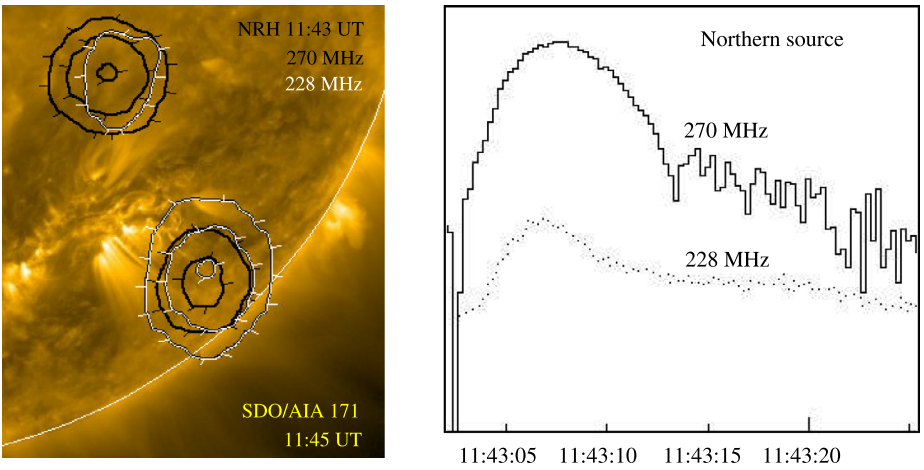

Figure 7 NRH source contours at 270 MHz (*black*) and 228 MHz (*white*) at 11:43:08 UT, plotted over an EUV image (*left*). The spectral feature is marked *1a* within group 1 bursts) in Figure 4. The flux curves (*on the right*) of the northern region show an enhancement at 270 MHz, which peaks later than the emission at 228 MHz. This suggests that the electron beam was moving down in the solar atmosphere. The later type III burst groups did not show this northern region again.

In between the type III bursts, we could also observe narrow-band radio spikes, identified as type I noise-storm structures (Figure 8). In high-resolution dynamic spectra, type I bursts appear as spot-like features, whereas vertical stripe-like features are type III bursts; see, for example, Mugundhan et al. (2018). The bandwidth of individual spikes was only 1 – 3 MHz. The spikes appeared in groups within a wider frequency range, between 80 and 50 MHz. These groups also drifted in frequency, typically towards higher frequencies.

Noise storm spikes are visible in the spectra also before our flare, appearing and growing stronger in intensity around 9:00 UT and lasting up to around 15:00 UT in the 80 – 50 MHz range. A GOES B3-class enhancement was observed at 09:00 – 09:45 UT, a possible sign of small-scale reconnection event(s). As type I noise storms are generally thought to be excited by plasma waves caused by non-thermal electrons trapped in closed magnetic-field lines, this suggests that there were a large number of non-thermal electrons present in the AR loops even before the start of our flare–CME event.

Near the start time of the first type III burst group, at 11:43 UT, some of the type III burst lanes seemed to split into two separate lanes. Figure 9 shows two of these V-shaped bursts in detail, observed by KAIRA (top spectrum, the slower-drift and turning lanes are indicated with arrows). The separation of electron-beam paths happens near 40 MHz, and the later, slower beam lanes disappear near 30 MHz. These frequencies correspond to solar atmospheric altitudes of $0.7 - 1.0\,R_{\odot}$, which are reasonable for large-scale loop heights and agree with the loops obtained with the PFSS model of the magnetic field, shown in Figure 2. Beam path curvature back towards higher frequencies, i.e. to higher densities, indicates that the electron beam follows magnetic field lines back to the Sun.

2.4. Coronal Mass Ejection

After the plasmoid ejection, a narrow dimming region started to appear in the EUV images, elongated towards the limb in the south-west direction. The SDO/AIA difference images are shown in Figure 10. A CME was first observed by the SOHO/LASCO-C2 coronagraph at

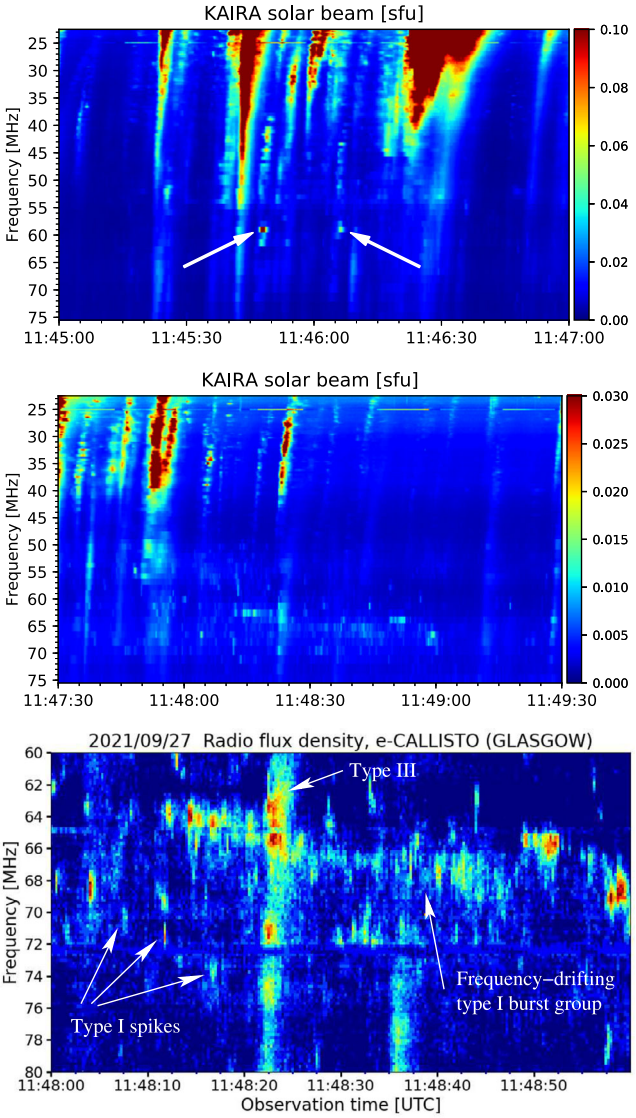

Figure 8 Dynamic spectrum taken during the second group of type III bursts show narrow-band enhanced plasma emission features, which are indicated with *arrows* in the KAIRA observations at 75 – 25 MHz (*top*). Narrow-band spikes (type I noise storm features) were observed in between the type III burst groups (KAIRA observations, *middle*). e-CALLISTO GLASGOW dynamic spectrum at 80 – 60 MHz shows the spikes and spike burst groups in more detail (*bottom*).

12:12:05 UT, when the CME leading front was located at a height of 2.57 $R_{\odot}$. The CME had a narrow angular width, 25 – 20 degrees (Figure 11), and it was propagating towards the south-west. There were no streamers located nearby the CME.

The CME speed from the first LASCO observations was ≈ 500 km s^{-1}, but the velocity decreased after the first hour and then stabilized to about 380 km s^{-1}, based on the linear fit

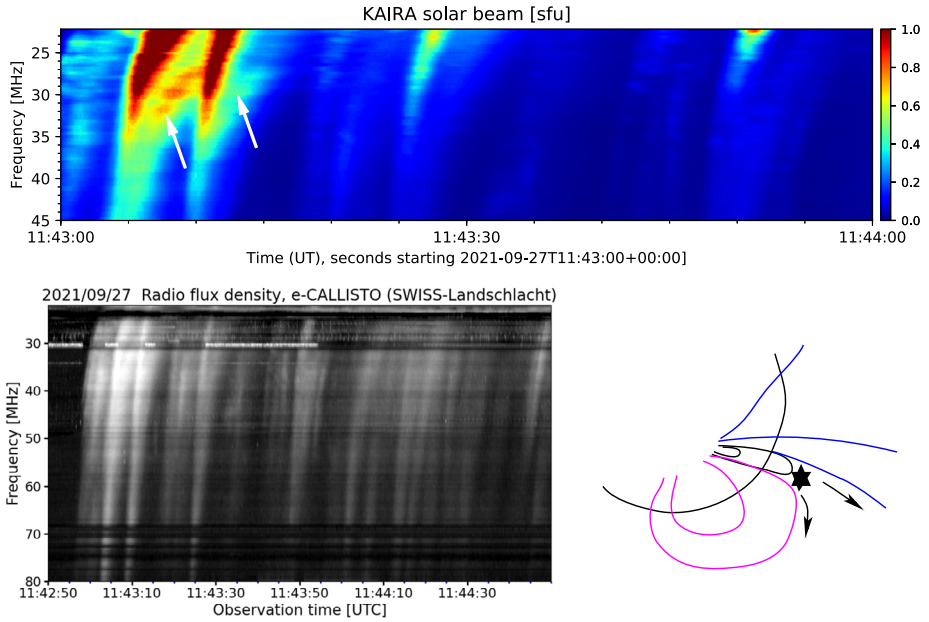

Figure 9 KAIRA observations of V-shaped type III bursts at 11:43 UT (*top*). *Arrows* point to the change in emission lane direction, visible at 35 – 27 MHz. The bursts were also observed by several *e-Callisto* stations; the dynamic spectrum shown here is from the SWISS-Landschlacht e-CALLISTO at 80 – 20 MHz (*bottom left*). Cartoon shows a possible configuration for the creation of V-shaped type III bursts. *Star* indicates reconnection, and *arrows* show the directions of two particle-beam paths, one along open field lines (emission with constantly decreasing frequencies) and the other following closed loops back to the Sun (emission lane turning back towards lower frequencies).

for the CME front heights available from the CME Catalog. The observed solar wind speed near Earth was 300 – 330 km s^{-1}, which explains some of the decrease in the CME speed.

We converted the CME heights to frequencies with the hybrid atmospheric-density model (Vršnak, Magdalenič, and Zlobec, 2004), which works well for the larger distances in the corona. These heights and frequencies are listed in Table 1, and they are shown in Figure 12.

3. Summary and Conclusions

The observed long-duration, metric type III burst emission that appeared as type III burst groups indicates continuous electron acceleration. If no high-frequency emission is observed at the same time, then it suggests that the acceleration region is located high in the corona (the higher the radio frequency, the lower the atmospheric height). The type III bursts that appeared in groups were formed at 200 MHz or nearby frequencies (corresponding to $\approx 0.15\,R_\odot$ or 100 Mm, heights above the solar surface as plasma frequency depends on electron density in the atmosphere), and each group had a duration of 2.5 – 1.5 minutes. These bursts did not look to have a direct, one-to-one correlation with hard X-ray count peaks (*Fermi*/GBM), but enhanced X-ray emission was observed during the type III burst group periods. As X-rays are the result of electrons colliding with denser structures, this can mean that part of the X-ray emission came from heating and part from particle acceleration.

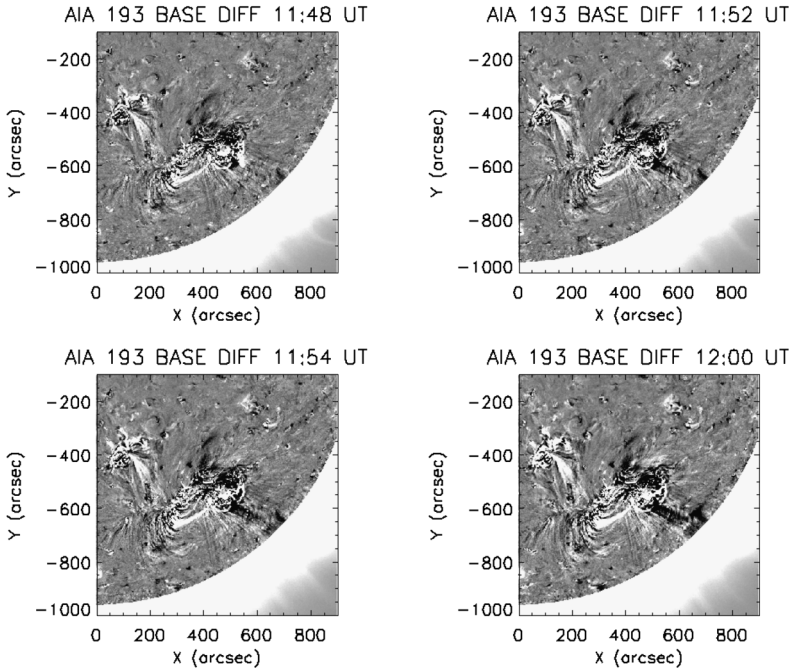

Figure 10 SDO/AIA 193 Å base-difference images (base at 11:32 UT). The narrow-width dimming region, located from the AR towards the south-west limb, matches with the type III burst regions imaged at 150 MHz, and also with the CME propagation direction.

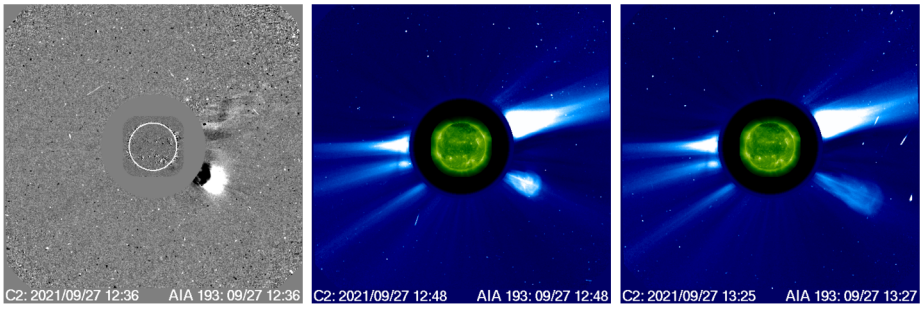

Figure 11 SDO/AIA 193 Å and SOHO/LASCO-C2 difference image at 12:36 UT (*left*), and direct AIA and C2 images at 12:48 UT (*middle*) and 13:25 UT (*right*). The CME was very compact and had a narrow width. No streamers were visible along the CME propagation path.

The unchanged start frequency (formation height) of each radio burst group suggests that the acceleration process of the burst particles was not due to reconnection in rising structures, but that the reconnecting fields remained at the same heights. A decrease in start frequency would indicate that the reconnection region is moving up in the atmosphere, where the density is lower. For example, Reiner et al. (2008) have suggested that in complex type III bursts the later electron acceleration can be the result of coronal reconfiguration, caused by, for example, an erupting CME.

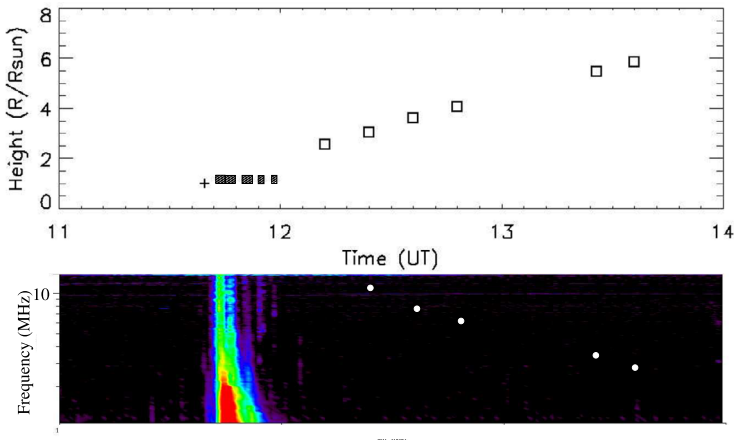

Figure 12 *Top*: CME leading front heights (*boxes*), the heights are from the LASCO CME Catalog, flare start time (*cross*), and metric type III burst group durations (*filled boxes*). *Bottom*: *Wind*/WAVES dynamic spectrum where *white circles* mark the CME leading front heights converted to frequencies with the hybrid atmospheric-density model.

Table 1 Heliocentric CME heights from LASCO-C2 observations converted to frequencies with the hybrid atmospheric-density model.

CME height [$R_\odot$]	Time [UT]	Frequency [MHz]
2.57	12:12:05	16.7
3.03	12:24:06	11.5
3.63	12:36:05	7.7
4.07	12:48:06	6.1
5.48	13:25:43	3.3
5.52	13:30:20	3.2
5.87	13:36:17	2.9

In Figure 9, we presented a possible configuration for the creation of type III bursts that show a split into two separate lanes at metric wavelengths. The observed split happened near 40 – 50 MHz, which corresponds to heights of $\approx 0.6 - 0.8\,R_\odot$ above the solar surface. The later, curved beam path can be explained by the large-scale loop shape and its slower rate of change in height, which becomes almost vertical later on. The "split" does not necessarily mean a physical split of the electron beam, but that part of the accelerated electrons gets access to field lines that curve to different directions, compared to those that propagate directly out along the open field lines. A similar split into two, "fast" and "slow" drifting burst parts, was reported also by Kallunki, McKay, and Tornikoski (2021). The burst they described was most probably associated with a CME that originated from the far side and had a narrow width in Earth view, and the true GOES-class was unknown and listed as a B-class flare.

Type III bursts with inverted-U and N-shaped emission lanes, observed at coronal heights, have been discussed by Démoulin et al. (2006). These burst shapes require large-scale loops and closed magnetic field lines, as in them the electron beams first travel upward along the field lines, then come back to lower heights, and in N-bursts the particles are mirrored back to larger heights. In our split V-shaped bursts, we did not find any evidence of mirroring, as the later branch simply faded away and ceased to be observed.

This high-altitude scenario resembles those presented by Heyvaerts, Priest, and Rust (1977) and Sterling and Moore (2001). In their models, there is a rising flux rope on the side of a coronal-hole open field, which reconnects ("external reconnection"). In our case, we have a large-scale loop on the side of open active-region field lines, with a rising but very narrow filament/plasmoid in between them. Due to the changes in the outflowing material, reconnection and particle acceleration are quasi-periodical. In this sense, the scenario is similar to loop–loop interactions, where the loop movements cause reconnection leading to oscillation in the radio emission. The many different possibilities for modulated reconnection have recently been described in Cattell et al. (2021).

The active region that produced the small, GOES B4.5-class flare on 27 September 2021 was surrounded by strong fields that guided the outflow of the ejected plasmoid. The CME had a very narrow width due to the small volume of plasma and the narrow tunnel-like exit path from the solar surface. This was observed in Figure 3, where the propagation direction of the long filamentary CME structure was changed, and it was bent along the fan-like field lines. The PFSS model also predicted large-scale loops that could come into contact with the ejected plasmoid. The metric type III burst groups could have been created by periodic reconnection, caused by coronal reconfiguration that affected the large-scale loops and the open field lines nearby. The type III bursts ended when the CME had lifted off and the material outflow had ceased.

Acknowledgements We thank the radio monitoring service at LESIA, Observatoire de Paris for providing value-added data that have been used for this study. We also thank the *e-Callisto* community for free access to their data and software. Our special thanks go to Kim Tolbert at GSFC, who prepared the *Fermi*/GBM response file manually for us, as the flare was not big enough for the quicklook procedure. KAIRA was funded by the University of Oulu and the FP7 European Regional Development Fund and is operated by the Sodankylä Geophysical Observatory with assistance from the University of Tromsø and volunteer effort. The CME catalog is generated and maintained at the CDAW Data Center by NASA and the Catholic University of America in cooperation with the Naval Research Laboratory. SOHO is a project of international cooperation between ESA and NASA.

Author contributions S. Pohjolainen prepared most of the solar images, radio images, X-ray plot, some of the radio spectral plots, and made the cartoon. D. McKay operates the Kilpisjarvi Atmospheric Imaging Receiver Array and prepared the KAIRA spectral plots. N.T. Sheshvan prepared the PFSS plot of the magnetic field structures. C. Monstein operates the international spectrometer-network e-Callisto and prepared most of the e-Callisto spectral plots. S. Pohjolainen wrote the main manuscript text and all authors revised the manuscript.

Funding Open Access funding provided by University of Turku (including Turku University Central Hospital).

Declarations

Competing interests The authors declare no competing interests.

References

Benz, A.O.: 2008, Flare observations. *Liv. Rev. Solar Phys.* **5**, 1. DOI.

Benz, A.O., Monstein, C., Meyer, H.: 2005, Callisto – a new concept for solar radio spectrometers. *Solar Phys.* **226**, 143. DOI.

Bougeret, J.-L., Kaiser, M.L., Kellogg, P.J., Manning, R., Goetz, K., Monson, S.J., Monge, N., Friel, L., Meetre, C.A., Perche, C., Sitruk, L., Hoang, S.: 1995, WAVES: the radio and plasma wave investigation on the wind spacecraft. *Space Sci. Rev.* **71**, 231. DOI.

Cairns, I.H., Lobzin, V.V., Donea, A., Tingay, S.J., McCauley, P.I., Oberoi, D., Duffin, R.T., Reiner, M.J., Hurley-Walker, N., et al.: 2018, Low altitude solar magnetic reconnection, type III solar radio bursts, and X-ray emissions. *Sci. Rep.* **8**, 1676. DOI.

Cattell, C., Glesener, L., Leiran, B., Dombeck, J., Goetz, K., Martínez Oliveros, J.C., Badman, S.T., Pulupa, M., Bale, S.D.: 2021, Periodicities in an active region correlated with type III radio bursts observed by Parker solar probe. *Astron. Astrophys.* **650**, A6. DOI.

Chen, X., Kontar, E.P., Chrysaphi, N., Jeffrey, N.L.S., Gordovskyy, M., Yan, Y., Tan, B.: 2020, Subsecond time evolution of type III solar radio burst sources at fundamental and harmonic frequencies. *Astrophys. J.* **905**, 43. DOI.

Démoulin, P., Klein, K.-L., Goff, C.P., van Driel-Gesztelyi, L., Culhane, J.L., Mandrini, C.H., Matthews, S.A., Harra, L.K.: 2006, Decametric N burst: a consequence of the interaction of two coronal mass ejections. *Solar Phys.* **240**, 301. DOI.

Gopalswamy, N.: 2016, History and development of coronal mass ejections as a key player in solar terrestrial relationship. *Geosci. Lett.* **3**, 8. DOI.

Hamini, A., Auxepaules, G., Birée, L., Kenfack, G., Kerdraon, A., Klein, K.-L., Lespagnol, P., Masson, S., Coutouly, L., Fabrice, C., Romagnan, R.: 2021, ORFEES – a radio spectrograph for the study of solar radio bursts and space weather applications. *J. Space Weather Space Clim.* **11**, 57. DOI.

Heyvaerts, J., Priest, E.R., Rust, D.M.: 1977, An emerging flux model for the solar phenomenon. *Astrophys. J.* **216**, 123. DOI.

Iwai, K., Miyoshi, Y., Masuda, S., Shimojo, M., Shiota, D., Inoue, S., Tsuchiya, F., Morioka, A., Misawa, H.: 2012, Solar radio type-I noise storm modulated by coronal mass ejections. *Astrophys. J.* **744**, 167. DOI.

Kallunki, J., McKay, D., Tornikoski, M.: 2021, First type III solar radio bursts of solar cycle 25. *Solar Phys.* **296**, 57. DOI.

Kawabata, Y., Iida, Y., Doi, T., Akiyama, S., Yashiro, S., Shimizu, T.: 2018, Statistical relation between solar flares and coronal mass ejections with respect to sigmoidal structures in active regions. *Astrophys. J.* **869**, 99. DOI.

Kerdraon, A., Delouis, J.M.: 1997, The Nançay Radioheliograph. In: Trottet, G. (ed.) *Coronal Physics from Radio and Space Observations*, *Lect. Notes Phys.* **483**, Springer, Berlin, 192. DOI.

Kontar, E.P., Chen, X., Chrysaphi, N., Jeffrey, N.L.S., Emslie, A.G., Krupar, V., Maksimovic, M., Gordovskyy, M., Browning, P.K.: 2019, Anisotropic radio-wave scattering and the interpretation of solar radio emission observations. *Astrophys. J.* **884**, 122. DOI.

Lecacheux, A.: 2000, The nançay decameter array: a useful step towards giant, new generation radio telescopes for long wavelength radio astronomy. In: Stone, R.G., Weiler, K.W., Goldstein, M.L., Bougerot, J.-L. (eds.) *Geophys. Mono. Ser.* **119**, 321. DOI.

Lemen, J.R., Title, A.M., Akin, D.J., Boerner, P.F., Chou, C., Drake, J.F., Duncan, D.W., Edwards, C.G., Friedlaender, F.M., Heyman, G.F., et al.: 2012, The Atmospheric Imaging Assembly (AIA) on the Solar Dynamics Observatory (SDO). *Solar Phys.* **275**, 17. DOI.

McKay-Bukowski, D., Vierinen, J., Virtanen, I.I., Fallows, R., Postila, M., Ulich, T., et al.: 2015, KAIRA: the Kilpisjärvi Atmospheric Imaging Receiver Array - system overview and first results. *IEEE Trans. Geosci. Remote Sens.* **53**, 1440. DOI.

Meegan, C., Lichti, G., Bhat, P.N., Bissaldi, E., Briggs, M.S., Connaughton, V., Diehl, R., Fishman, G., Greiner, J., Hoover, A.S., et al.: 2009, The Fermi gamma-ray burst monitor. *Astrophys. J.* **702**, 791. DOI.

Mercier, C., Subramanian, P., Chambe, G., Janardhan, P.: 2015, The structure of solar radio noise storms. *Astron. Astrophys.* **576**, A136. DOI.

Mondal, S., Oberoi, D.: 2021, Insights from snapshot spectroscopic radio observations of a weak type I solar noise storm. *Astrophys. J.* **920**, 11. DOI.

Monstein, C., Csillaghy, A., Benz, A.O.: 2023, CALLISTO Solar Spectrogram FITS files [Data set]. *International Space Weather Initiative (ISWI)*. DOI.

Mugundhan, V., Ramesh, R., Kathiravan, C., Gireesh, G.V.S., Hegde, A.: 2018, Spectropolarimetric observations of solar noise storms at low frequencies. *Solar Phys.* **293**, 41. DOI.

Newkirk, G. Jr.: 1961, The solar corona in active regions and the thermal origin of the slowly varying component of solar radio radiation. *Astrophys. J.* **133**, 983. DOI.

Nindos, A., Aurass, H., Klein, K.-L., Trottet, G.: 2008, Radio emission of flares and coronal mass ejections. Invited review. *Solar Phys.* **253**, 3. DOI.

Pick, M., Vilmer, N.: 2008, Sixty-five years of solar radioastronomy: flares, coronal mass ejections and Sun–Earth connection. *Astron. Astrophys. Rev.* **16**, 1. DOI.

Pohjolainen, S., van Driel-Gesztelyi, L., Culhane, J.L., Manoharan, P.K., Elliott, H.A.: 2007, CME propagation characteristics from radio observations. *Solar Phys.* **244**, 167. DOI.

Reid, H.A.S., Vilmer, N.: 2017, Coronal type III radio bursts and their X-ray flare and interplanetary type III counterparts. *Astron. Astrophys.* **597**, A77. DOI.

Reiner, M.J., Klein, K.-L., Karlicky, M., Jiricka, K., Klassen, A., Kaiser, M.L., Bougeret, J.-L.: 2008, Solar origin of the radio attributes of a complex type III burst observed on 11 April 2001. *Solar Phys.* **249**, 337. DOI.

Roberts, J.A.: 1959, Solar radio bursts of spectral type II. *Austral. J. Phys.* **12**, 327. DOI.

Sterling, A.C., Moore, R.L.: 2001, Internal and external reconnection in a series of homologous solar flares. *J. Geophys. Res.* **106**, 25227. DOI.

Vršnak, B., Magdalenič, J., Zlobec, P.: 2004, Band-splitting of coronal and interplanetary type II bursts. III. Physical conditions in the upper corona and interplanetary space. *Astron. Astrophys.* **413**, 753. DOI.

Vršnak, B., Sudar, D., Ruždjak, D.: 2005, The CME-flare relationship: are there really two types of CMEs? *Astron. Astrophys.* **435**, 1149. DOI.

Warmuth, A.: 2007, Large-scale waves and shocks in the solar corona. In: Klein, K.L., MacKinnon, A.L. (eds.) *The High Energy Solar Corona: Waves, Eruptions, Particles*, *Lect. Notes Phys.* **725**, 107. DOI.

Wuelser, J.-P., Lemen, J.R., Tarbell, T.D., Wolfson, C.J., Cannon, J.C., Carpenter, B.A., Duncan, D.W., Gradwohl, G.S., Meyer, S.B., Moore, A.S., et al.: 2004, EUVI: the STEREO-SECCHI extreme ultraviolet imager. In: Fineschi, S., Gummin, M.A. (eds.) *EUVI: The STEREO-SECCHI Extreme Ultraviolet Imager*, *Proc. SPIE* **5171**, 111. DOI.